19A.4 USING WINDS FROM THE 4-D VARIATIONAL DOPPLER RADAR ANALYSIS SYSTEM (VDRAS) TO NOWCAST CONVECTION IN TAIWAN

Amanda R. S. Anderson, James W. Wilson, Tracy Emerson,
Zhuming Ying, Juanzhen Sun, Rita D. Roberts
Nation Center for Atmospheric Research, Boulder, Colorado, USA

1. INTRODUCTION

The complex terrain of Taiwan presents a difficult problem in nowcasting the initiation of convection in the country. The National Center for Atmospheric Research (NCAR) has been collaborating with the Taiwan Central Weather Bureau (CWB) to research heavy rainfall-producing convection on the island, specifically related to predicting initiation of such storms, and transfer/tune the AutoNowCaster (ANC) system to aid in nowcasting this convection.

The ANC is an expert system that produces rapidly updating, one-hour nowcasts of thunderstorm initiation, growth, and decay (Mueller et al. 2003). The system ingests model data, surface observations, satellite, and radar data. These data are processed and run through a system of fuzzy logic equations and weights to produce one-hour interest field nowcasts that update approximately every five minutes. In addition to these data, forecaster input is an essential component of the system and is being tested as part of the Forecaster Over the Loop (FOTL) project (Roberts et al. 2005). In addition to the testing occurring in the United States, NCAR is refining and testing the ANC in Taiwan for the purpose of predicting heavy rainfall.

In the complex terrain of Taiwan, wind direction and magnitude have a significant impact on the formation and location of convection and heavy rainfall (Chen and Chen 2003). Accurate wind analyses are essential for systems such as the ANC to make useful nowcasts. To this end, the Variation Doppler Radar Analysis System (VDRAS; Sun and Crook, 2001) is used within the ANC to provide predictors related to the wind field.

Initial observations with VDRAS winds over Taiwan show that in synoptically forced, widespread rainfall situations, VDRAS has enough radar data to perform a representative analysis of the wind field, including some smaller-scale wind shifts that may impact where more intense storms form (Anderson et al. 2010). However, wind direction plays an especially important role in cases where the synoptic forcing is weak, and local forcings are the primary indication of where and when storms will initiate (e.g., Akaeda et al. 1995).

To best incorporate wind analyses into the ANC for nowcasting heavy rainfall-producing convection, VDRAS was run for 17 cases during the Southwest Monsoon Experiment/Terrain-influence Monsoon Rain Experiment (SoWMEX/TiMREX; Jou et al. 2010), and the resulting wind fields compared to both observed data as well as initiation locations.

2. DATA AND METHODS

The SoWMEX/TiMREX field project was conducted jointly between the United States and Taiwan during the 2008 monsoon season in southwestern Taiwan (May-June). Many cases during this period involved the Mei-Yu front, which was a focus of the experiment (Chen 2004; Ciesielski et al. 2010), and past work has indicated that VDRAS performs well during such cases, where widespread rain provides ample radar velocity data for analysis (Anderson et al. 2010), and such analyses can be useful for detecting convective initiation (Sun et al. 2010). Winds become especially important in cases of weak synoptic-scale forcing, where local circulations play a large role. To examine VDRAS's performance and utility for such cases, 17 days of weak synoptic-scale forcing were chosen from the SoWMEX/TiMREX dataset (Table 1).

VDRAS is a 4-D variational assimilation system that produces frequently updated (on the order of 10 minutes) analyses using Doppler radar, surface observations, and a mesoscale model background (Sun and Crook, 2001). The mesoscale model is used to represent motion in the atmosphere, and then Doppler radar velocities are assimilated as well as surface observations to produce the VDRAS analysis. For this study, a Weather Research and Forecasting (WRF; Skamarock et al. 2005) simulation was used as the background field. Radar data was assimilated from two radars: the NCAR S-Pol polarimetric research radar (Keeler et al. 2000) that was set up for the field project and the operational Taiwanese RCCG radar at Chi-Gu (Fig. 1). Both radars operate at S-band. Surface data was also assimilated into VDRAS to produce the final wind fields.

Table 1: Summary of weak synoptic forcing cases used in analysis.

Case	Initiation Period (UTC)	# of Cells
17 May	0351-0843	9
23 May	0734-0942	25
24 May	0600-1107	10
25 May	0259-1130	96
26 May	0107-0852	69
01 Jun	0322-0805	26
07 Jun	0637-0845	8
08 Jun	0222-1845	37
09 Jun	0230-2322	27
10 Jun	0122-0715	7
12 Jun	0515-1100	42
13 Jun	0307-0937	67
18 Jun	0337-0937	23
19 Jun	0539-1352	35
20 Jun	0552-1015	5
21 Jun	n/a	0
23 Jun	n/a	0

Initiation times and locations were identified on each of the days using S-Pol data and the Thunderstorm Identification, Tracking, Analysis, and Nowcasting (TITAN) algorithm (Dixon and Wiener 1993). TITAN drew a polygon around a cell provided it had reflectivity between 35 and 100 dBZ, was greater than 10 km^3 in echo volume, and persisted more than one radar scan. If the cell had actually reached 35 dBZ but was not detected by TITAN until later due to being too small in size, the earlier initiation time was used. Two cases with no initiation (21 June and 23 June) were included in the analysis to identify differences between weakly-forced days that did and did not produce convection.

In addition to the VDRAS and Doppler radar data, observations from the National Central University Integrated Sounding System (NCU ISS) wind profiler were compared to the VDRAS winds to examine how well VDRAS represented the environment near the profiler. The NCU ISS wind profiler was located at the SoWMEX/TiMREX supersite at Guanxin elementary school (TIMREX Operations Plan; Fig. 1). This profiler operates at 915 MHz (Cielsielski et. al. 2010) and reported data in both high mode (up to 9.4 km AGL at 0.238 km increments) and low mode (up to 4.9 km AGL at 0.098 km increments). The high mode was used in this analysis. Note that there are substantial amounts of missing data, particularly in the upper levels, which makes comparisons difficult at certain times and heights.

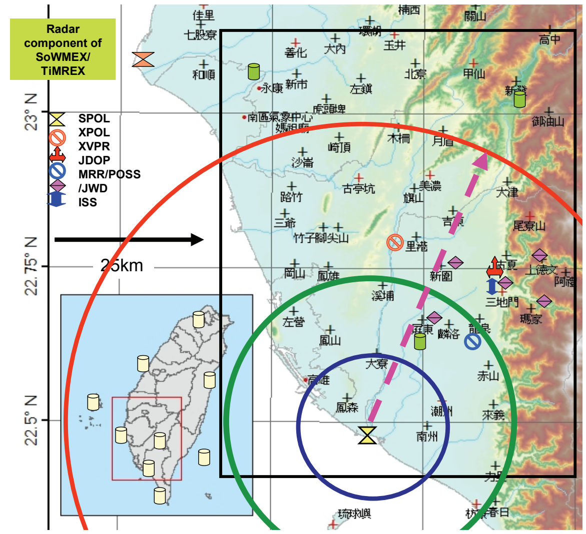

Figure 1: Overview of surface observation network. S-Pol is located at the yellow hourglass, RCCG at the red hourglass, and the wind profiler at the blue arrows labeled ISS. From Jou et al. (2010).

The VDRAS winds were first examined in the context of initiation time and location patterns to determine if a consistant trend existed that could be incorporated as an ANC interest field (Section 3). VDRAS winds were then compared with the NCU ISS wind profiler to assess how well VDRAS was representing the winds in this location and whether subtle shifts in wind that could increase initiation prediction were being missed at the resolution in which VDRAS was run (Section 4).

3. EXAMINATION OF VDRAS WINDS AS PREDICTORS OF INITIATION

Overall, on the weak synoptically forced days, initiation tended to occur just to the west of the Central Mountain Range (CMR) and west of where VDRAS usually indicated the strongest convergence was occurring. There were also indications that the storms may be occurring in areas of upslope flow, although the existence of upslope flow was not sufficient for producing storms (Fig. 2).

The typical wind conditions across the entire VDRAS domain were examined to see if the

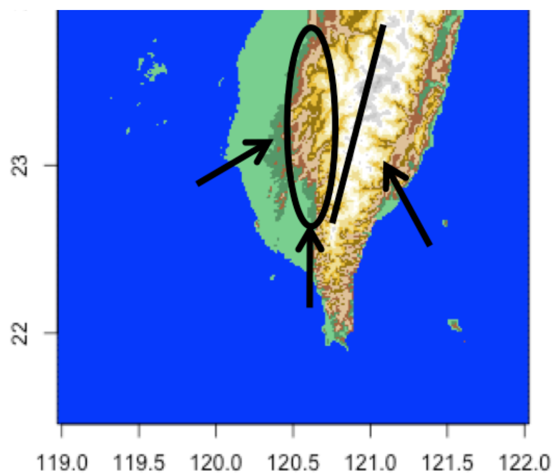

Figure 2: Schematic of typical conditions in southwestern Taiwan for weak synoptic forcing cases. Typical VDRAS wind direction is shown by arrows, largest VDRAS convergence is shown by line, and typical initiation zone is circled.

overall pattern of the wind, as analyzed by VDRAS, could be used to produce climatological maps of initiation locations that could subsequently be used as interest fields in the ANC. Frequencies of wind direction and speed showed no consistency between initiation patterns on different days (Table 2). Likewise, combining both direction and speed through the use of wind roses for each case did not show any consistent trends (Fig. 3).

To narrow down the analysis from the whole-domain examinations above, time series of VDRAS wind speed and direction were produced for each initiation location. Overall, wind speeds tended to stay steady or increase leading up to initiation with fewer instances of decreasing speed, but there was not enough separation between these categories to develop a concrete conclusion (Table 3). Likewise, wind direction did not exhibit any clear trends when veering/backing and trending towards a more

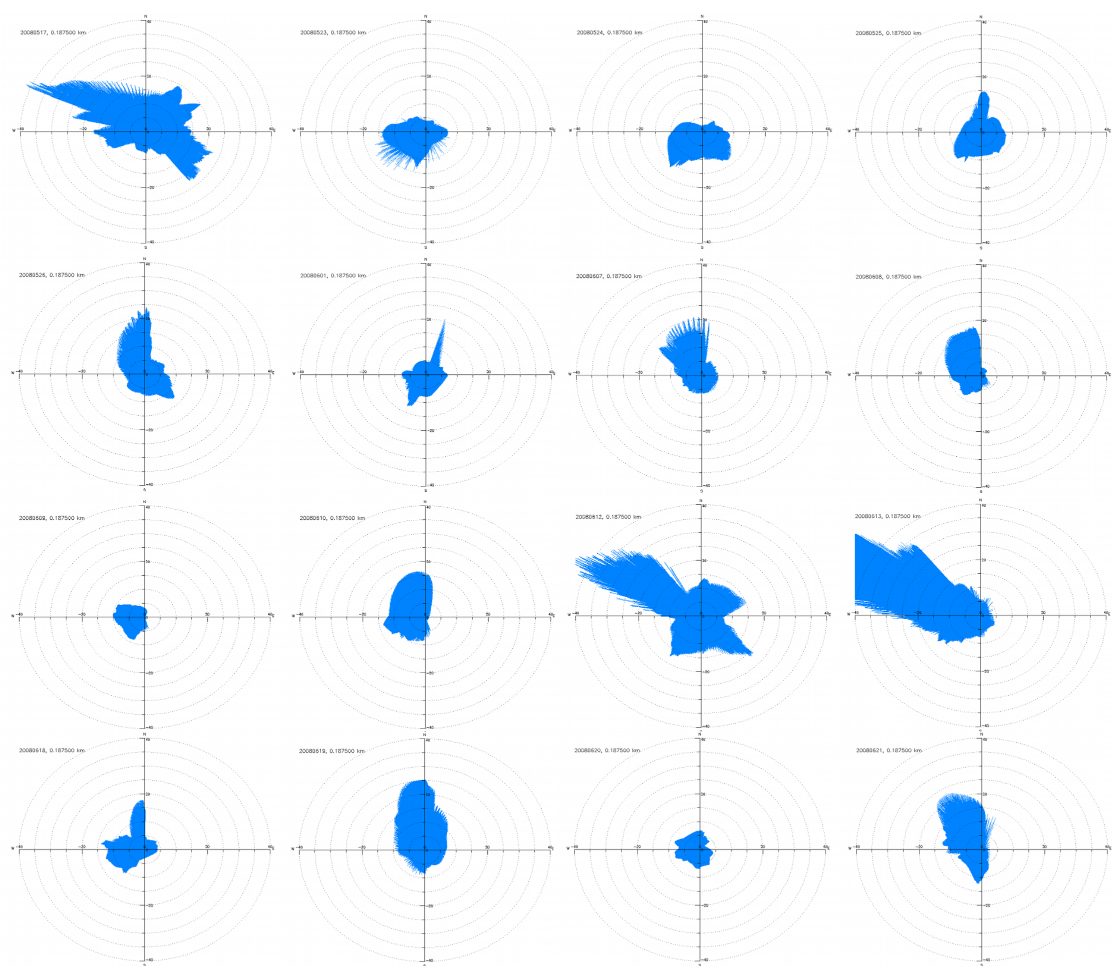

Figure 3: Wind roses for all cases, ordered chronologically from left to right, top to bottom (23 June not shown).

westerly wind were examined (Table 3), although there were more instances of a more westerly wind trending than either steady or less westerly, possibly reflecting the upslope flow observed overall as most initiation occurred along the western slopes of the CMR.

Table 2: VDRAS wind speed and direction frequency maxima at lowest VDRAS level (0.1875 km). If more than one dominant direction was observed, most frequent direction is listed first with following unordered.

Case	Speed (m s^{-1})	Direction
17 May	5-10	N
23 May	0-5	S/SW
24 May	0-10	SW/W
25 May	0-5	SW/W
26 May	0-5	SW/W/NW
01 Jun	0-5	SW/W/N
07 Jun	0-5	S/SE
08 Jun	0-10	S
09 Jun	5-10	S
10 Jun	5-10	S/SW
12 Jun	0-5	SW/S
13 Jun	5-10	S/SW
18 Jun	0-10	S
19 Jun	0-5	SW/S/SE/E
20 Jun	0-5	SW/S/SE
21 Jun	0-5	SW/SE/W
23 Jun	0-10	S/SE

Table 3: Counts of VDRAS wind speed and direction changes prior to initiation for lowest VDRAS level (0.1875 km). "Less Veering" indicates wind backed.

	More	Steady	Less
Speed	87	168	60
Veering	126	108	77
Westerly	142	78	91

As indicated above, there were no patterns identified across the VDRAS domain and all cases that could be used confidently to develop interest fields for the ANC. However, it is important to note that the quality of the data ingested by VDRAS varied between days, with the best data available for the 1 June and 7 June cases. These two cases were examined separately to see if any patterns were noticeable using the highest quality VDRAS runs.

On 1 June, initiation began over the western slopes of the CMR around 0330 UTC following a steady turning of the winds over the plains to westerly. Storms continued to initiate in the upslope flow through about 0930 UTC. Winds over the plains had shifted slightly more northwest.

On 7 June, winds began shifting from northerly to westerly over the plains and increased in speed leading up to initiation around 0700 UTC over the western slopes of the CMR. Initiation was confined to the northern part of the S-Pol domain. Winds in the southern area along the slopes had more of a southerly component and therefore not as much upslope was occurring as in the initiation areas to the north. Storms moved away or died off by 0940 UTC.

Initiation locations for these two cases were similar, although initiation extended further south on 1 June than 7 June (Fig. 4). A comparison of wind directions shows a more westerly component on 1 June as opposed to the more southerly component on 7 June (Fig. 5). If upslope flow were an important contributor to initiation, then the more southerly flow on 7 June may be a reason why there was no initiation along the north-south oriented terrain on 7 June while there was initiation there on 1 June. There were also more instances of winds >10 m s^{-1} on 7 June compared to 1 June in the layer from about 2.8 km to 7.3 km AGL (Fig. 6). However, this speed difference was not consistent across all cases when trying to relate overall wind speed to frequency of initiation.

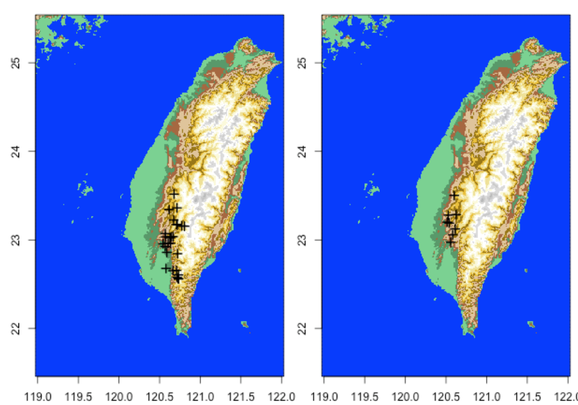

Figure 4: Initiation locations (black crosses) on 1 June (left) and 7 June (right).

Overall, the VDRAS wind patterns did not vary consistently between different initiation times and locations across the cases, although there were some indications that upslope flow along the western slopes of the CMR may contribute to initiation on weakly forced days. This effect is being explored for inclusion in the

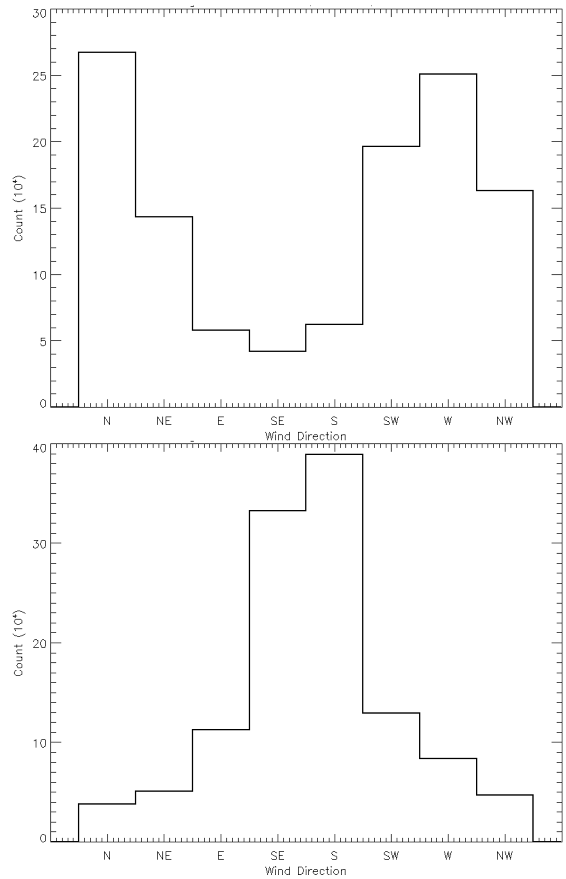

Figure 5: Wind direction histograms for 1 June (top) and 7 June (bottom) for lowest VDRAS level (0.1875 km AGL).

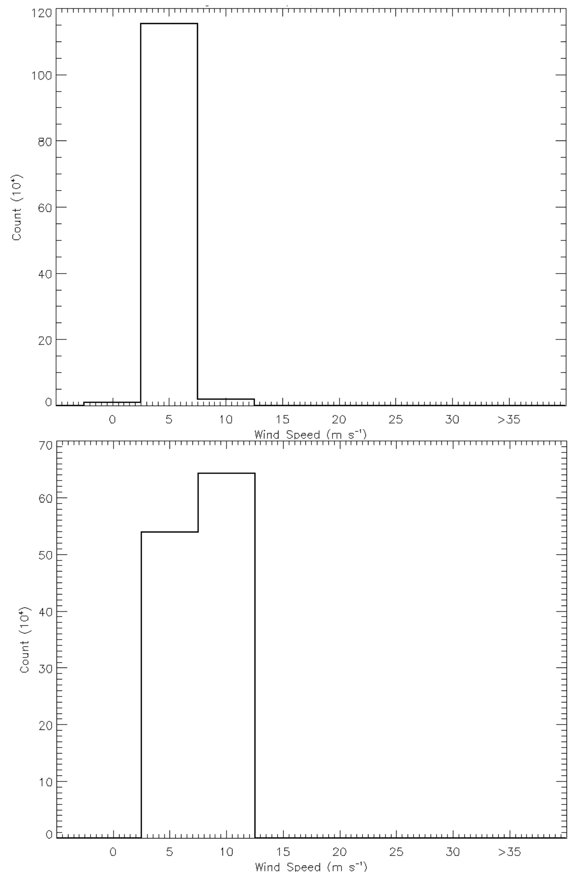

Figure 6: Wind speed histograms for 1 June (top) and 7 June (bottom) at VDRAS level 5.0625 km AGL.

ANC through the use of a simple model that will calculate vertical motion along the terrain given the analyzed wind direction and speed from VDRAS.

4. COMPARISON OF VDRAS ANALYSES AND WIND PROFILER OBSERVATIONS

As mentioned in the previous section, input data quality varied among the cases, and it is possible that the lack of conclusive patterns across these cases could be due, in part, to improperly analyzed winds. To assess VDRAS's ability to capture local circulations along the western slopes of the CMR, the analyses were compared to observations made by the NCU ISS wind profiler located at the SoWMEX/TiMREX supersite. The closest VDRAS grid point to the wind profiler was identified, and then the VDRAS winds were linearly interpolated to the time and height coordinates of the wind profiler in the same method as Anderson et al. (2010).

Several cases matched poorly with the wind profiler observations, particularly the May cases and late June cases (19 June – 23 June; Fig. 7). The early June cases matched more closely, including 1 June and 7 June, which were identified as having the best input data. For the lowest levels, VDRAS tended to have direction differences on the order of 40-70 degrees for the less well-matched cases and around 20-40 degrees for better-matched cases (Fig. 7). Considering the importance of terrain, along with upslope that would occur with westerly winds, these large wind differences could lead to VDRAS not capturing terrain-induced convection as well as direct observations would. Speed differences were less of an issue, with differences generally around 0-5 m s^{-1}.

Overall, the VDRAS winds had substantial differences in direction compared to the wind profiler. This could indicate that VDRAS is not capturing the local wind flow along the terrain properly, leading in part to the ineffectiveness of finding patterns in the VDRAS winds in terms of initiation locations.

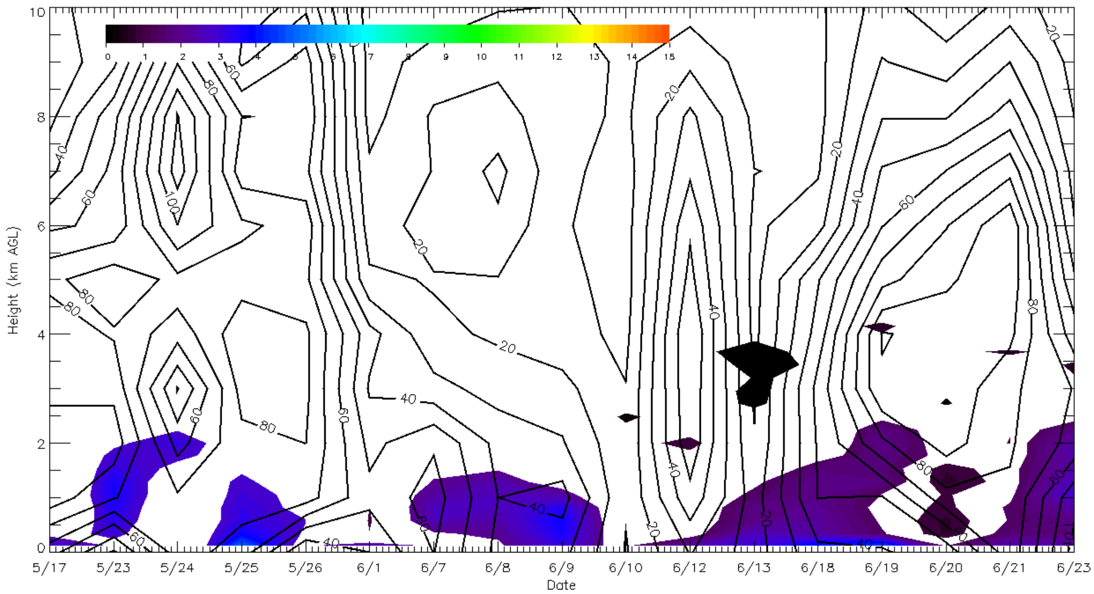

Figure 7: Mean absolute difference (MAD) between VDRAS and wind profiler wind speeds (filled) and directions (contoured) by case and height. MAD is similar to mean absolute error (MAE), except no "truth" value is assumed, and therefore only a difference between two values is considered, rather than the error of one.

5. CONCLUSIONS

On weak synoptic forcing days, local wind circulations in the complex terrain of Taiwan likely play an important role in where and when initiation occurs. To explore how to make use of wind information in the ANC, VDRAS wind fields from such days were explored in the context of initiation times and locations.

Across the VDRAS domain, there were no consistent patterns in the VDRAS wind fields that could be used to produce interest fields of initiation location in the ANC. There was evidence of upslope flow along the western slopes of the CMR, but this was a broad inference rather than a specific predictor of initiation. Therefore, it would be difficult at this point to produce interest maps, such as climatological maps of initiation location, based on larger-scale wind flow patterns alone.

Some cases had better input data (radar and surface observations) than others. The two cases with the best input data, 1 June and 7 June, again only showed some upslope flow.

Comparing the VDRAS winds in the vicinity of the supersite with the wind profiler showed that some cases matched better with the observed winds than others. Across all cases, VDRAS tended to show different wind directions than the wind profiler. This could be a reason why no specific wind predictors were found with VDRAS, as the resolution may have been too coarse to properly resolve local circulations.

In addition to the resolution, the small wind speeds occurring on these weakly forced days could cause errors in the calculated wind direction in VDRAS. VDRAS errors tend to be on the order of 2–3 m s^{-1} (Sun and Crook 2001). If the winds themselves are on the order of 2–3 m s^{-1}, this could lead to a wind direction quite different from that observed, though this effect is unlikely when winds quicken to 5 m s^{-1}. Some of the errors seen in the wind profiler comparisons may also have been due to slight spatial errors in wind shifts.

Although this study was unable to identify the best way to incorporate VDRAS-analyzed winds into the ANC to nowcast initiation on weakly-forced days, there are more facets of VDRAS that remain to be examined. Future work includes a closer examination of the role of upslope using the wind profiler and S-Pol velocities as well as running one of the cases at a higher resolution (such as 1 km) to see if VDRAS can resolve any additional features. VDRAS winds will also be used to calculate updrafts resulting from interaction with the terrain, which may provide more information about the upslope components presented in this paper. Finally, VDRAS also produces other fields, such as temperature perturbation, that could be useful in predicting initiation within the ANC on days with weak synoptic forcing.

6. REFERENCES

Akaeda, K., J. Reisner, and D. Parsons, 1995: The role of mesoscale and topographically induced circulations initiating a flash flood observed during the TAMEX project. Mon. Wea. Rev., 123, 1720–1739.

Anderson, A.R.S., J. Sun, R. Roberts, W-C. Lee, 2010: A comparison of SoWMEX/TiMREX wind observations with WRF and VDRAS 3-D wind fields on 31 May 2008. *Extended Abstracts, 3rd SoWMEX/TiMREX Science Workshop*, Taipei, Taiwan, Taiwan Weather Research Program, 4.2.

Chen, C.-S., Y.-L. Chen, 2003: The Rainfall Characteristics of Taiwan. *Mon. Wea. Rev.*, **131**, 1323–1341.

Chen, G.T.J., 2004: Research on the phenomena of Meiyu during the past quarter century: An overview. *East Asian Monsoon*, C. P. Chang, Ed., Series for Meteorology of East Asia, Vol. 2, World Scientific, 357–403.

Ciesielski, P.E., and Coauthors, 2010: Quality-Controlled Upper-Air Sounding Dataset for TiMREX/SoWMEX: Development and Corrections. *J. Atmos. Oceanic Technol.*, **27**, 1802–1821.

Dixon, M., and G. Wiener, 1993: TITAN: Thunderstorm identification, tracking, analysis, and nowcasting—A radar-based methodology. *J. Atmos. Oceanic Technol.*, **10**, 785–797.

Jou, B.J.-D., W.-C. Lee, and R.H. Johnson, 2010: An overview of SoWMEX/TiMREX. *Selected Papers of the Fourth International Monsoon Workshop*, C.P. Chang, Ed., World Scientific, 1–16.

Keeler, R.J., J. Lutz, and J. Vivekanandan, 2000: S-POL: NCAR's polarimetric Doppler research radar. Preprints, *IGARSS-2000*, Honolulu, HI, IEEE, 1570–1573.

Mueller, C., T. Saxen, R. Roberts, J. Wilson, T. Betancourt, S. Dettling, N. Oien, J. Yee, 2003: NCAR Auto-Nowcast System. *Wea. Forecasting*, **18**, 545–561.

Roberts, R., S. Fano, W. Bunting, T. Saxen, E. Nelson, C. Mueller, D. Megenhardt, D. Albo, S. Dettling, A. Crook, N. Oien, H. Cai, K. Johnston, S. Smith, M. Ba, and T. Amis, 2005: The NWS/NCAR Man In The Loop (MITL) Nowcasting Demonstration: Forecaster Input into a Thunderstorm Nowcasting System. *Proc. WWRP Symp. Nowcasting & Very Short Range Forecasting*, Toulouse, France, 5-9 September, 7.26.

Skamarock, W.C., J.B. Klemp, J. Dudhia, D.O. Gill, D.M. Barker, W. Wang, and J.G. Power, 2005: A description of the advanced research WRF version 2. NCAR Tech. Note TN-468+STR, 88 pp.

Sun, J., N.A. Crook, 2001: Real Time Low-Level Wind and Temperature Analysis Using Single WSR-88D Data. *Wea. Forecasting*, **16**, 117–132.

Sun, J., M. Chen, Y. Wang, 2010: A frequent-updating analysis system based on radar, surface, and mesoscale model data for the Beijing 2008 Forecast Demonstration Project. *Wea. Forecasting*, **25**, 1715–1735.

Taiwan Island Monsoon Rainfall Experiment (TIMREX) Operations Plan.